Macromolecules
ARTICLE

Macromolecules **2010**, *43*, 9401–9410 **9401**
DOI: 10.1021/ma102205t

High Crystallinity and Nature of Crystal−Crystal Phase Transformations in Regioregular Poly(3-hexylthiophene)

Ovidiu F. Pascui,[†] Ruth Lohwasser,[‡] Michael Sommer,[‡] Mukundan Thelakkat,[‡] Thomas Thurn-Albrecht,[†] and Kay Saalwächter*,[†]

[†]*Institut für Physik, Martin-Luther-Universität Halle-Wittenberg, D-06099 Halle, Germany, and* [‡]*Angewandte Funktionspolymere, Makromolekulare Chemie I, Universität Bayreuth, 95440 Bayreuth, Germany*

Received September 23, 2010; Revised Manuscript Received October 1, 2010

ABSTRACT: Molecular weight and stereoregularity affect the morphology and the crystallinity of conjugated polymers and are thus of pivotal relevance for the mobility of charge carriers in electro-optical device applications. Currently, poly(3-akylthiophenes) are discussed as one of the most promising classes of materials for photovoltaic applications. Here, we use ^{13}C solid-state NMR to determine the crystallinity and details on crystal−crystal phase transformations in regioregular head-to-tail poly(3-hexylthiophene) of well-defined molecular weight and demonstrate that the crystallinity was previously severely underestimated. Typical crystallinities are at least around 37% for the lowest molecular weights and as high as about 64% upon increasing MW, corresponding to a corrected maximum value for the reference melting enthalpy of $\Delta H_m^\infty \approx 37$ J/g for use in DSC experiments. Using 1D ^{13}C spectra and 2D experiments that measure the strength of ^{13}C−^{1}H dipolar couplings, we observe that the crystal−crystal phase transition between a 3D- and a 2D-ordered crystalline phase at around 60 °C entails a structural disordering process of the alkyl side chains, while not affecting rigidity and conformation of the backbones. This phase transition is suppressed at higher molecular weights due to a kinetic suppression of the formation of the alkyl-ordered low-temperature phase.

Introduction

Conjugated polymers such as poly(3-alkylthiophenes), P3ATs, have attracted considerable interest due to their semiconducting properties, resulting in potential application in organo-electronic devices like light-emitting diodes (LED), organic field-effect transistors (OFET), and photovoltaic cells.[1−3] The solubility, fusibility, and stability of these semiconducting conjugated polymers render them easily processable,[4] enabling the production of printed electronics on flexible substrates. The electronic and optical properties of polymeric alkylthiophenes depend strongly on the stereoregularity,[5−7] solvent,[7] and molecular weight (MW) of the sample.[8−13] Varying the MW by 1 order of magnitude results in a 4 orders of magnitude change in the mobility of the charge carriers in the sample.[10] This effect is at least to a large extent related to the corresponding changes in crystallinity.[9,14−16] Accordingly, the charge carrier mobility at room temperature is almost 3 orders of magnitude higher for highly regular (98%) head−tail, P3HT as compared with that of samples with lower HT content (81%),[5] while for even more irregular samples, the electronic conductivity drops by another factor of 20−50.[17−19] The regioregularity, i.e., the percentage of stereoregular head-to-tail (HT) attachments of the alkyl side chains to the 3-position of the thiophene ring,[17] is controlled by the nature of the catalyst used for polymerization. In recent years, more and more refined synthetic methods were developed to produce highly regioregular P3ATs with high reproducibility,[17,20,21] and correspondingly the quality of the investigated materials constantly improved.

P3HT is a semicrystalline polymer, and its crystalline structure is highly anisotropic. It exhibits $\pi-\pi$ stacking of the planar backbones in the *b* direction and a larger scale nanophase-separated structure in the *a* direction caused by segregation between main and side chains as shown in Figure 1.[22,23] The unit cell is commonly described as orthorhombic, and more detailed investigations show deviations pointing at a monoclinic[9] structure. Winokur et al.[24] initially suggested a structure with disordered side chains[25] in the otherwise crystalline material. Later, the presence of tilting of the side chains[26] and, recently,[27] evidence for the existence of interdigitated and tilted but disordered side chains were reported for P3ATs with long alkyl chains. While the melting of the side chains at high temperature in P3ATs with longer alkyl chains was observed by DSC previously,[28,29] clear evidence for a separate side-chain melting taking place in P3HT was obtained only recently based on combined DSC and X-ray scattering results.[30] These experiments gave evidence for a corresponding phase transition around 60 °C and were obtained on a P3HT sample with defined molecular weight and high regioregularity. Side-chain melting gives rise to a loss of correlation between neighboring layers of main chains (in *a* direction). Figure 2 shows a schematic presentation of the structure in the corresponding phases. These results suggest that P3HT is a highly heterogeneous material in terms of molecular packing and mobility.

Given the strong correlation between mobility of the charge carriers and molecular weight, mostly caused by structural features, our knowledge about the exact structure of P3HT is rather limited. Presently, there is no reliable method to determine the crystallinity of a given sample of P3HT. There is evidence that the extrapolated value for ΔH of 100% crystalline P3HT given in ref 23 is significantly too large.[30] A calibration for crystallinity based on scattering experiments is not available. Additionally, the situation in a material like P3HT is rather complex, as in addition to the fact that there are crystalline and amorphous parts in the sample, the possibility has to be taken into account that main chains and side chains display different degrees of order. Information about the latter question can only indirectly be obtained from

*Corresponding author. E-mail: kay.saalwaechter@physik.uni-halle.de.

Published on Web 10/21/2010

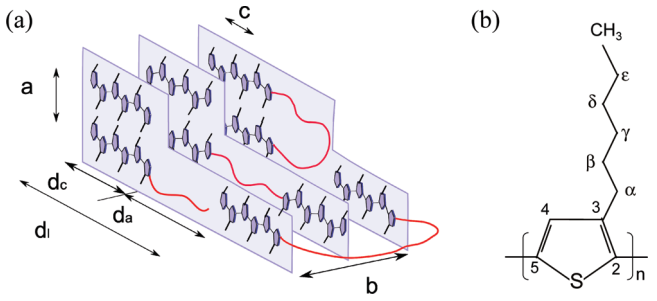

Figure 1. (a) Typical microstructure of regioregular P3HT, with curvy lines representing segments in the amorphous domain. Crystal lattice parameters **a**, **b**, **c**; thickness of the lamellar crystals d_c; thickness of the amorphous layers d_a; long period $d_l = d_a + d_c$. (b) Numbering scheme of the carbons in the repeat unit of P3HT.

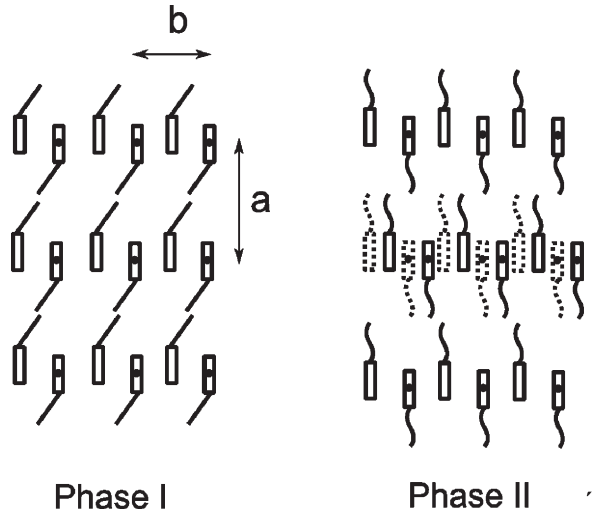

Figure 2. Schematic of phases I and II. Low temperature: regular 3D-crystal with ordered main and side chains. High temperature: regular packing of the main chains only. The side chains are molten and disordered. Correspondingly different main-chain layers lose correlation with each other as illustrated for the central layer.

scattering experiments, while solid-state NMR, as a local technique, promises to supply additional information.

NMR methods have been applied to investigate several aspects of P3AT's. Liquid-state NMR, on the one hand, is an indispensable tool in determining the stereo/regioregularity of P3HT, including ^{1}H and ^{13}C signal assignments.[20,28,29,31] Solid-state NMR, on the other hand, was used to analyze the molecular dynamics in regioregular poly(3-butylthiophene), P3BT, and poly(3-dodecylthiophene), P3DDT, close to the glass transition temperature.[32] Bolognesi et al. used nonquantitative ^{13}C MAS NMR spectra to analyze the thermal behavior of the poly(3-octylthiophene), P3OT. The existence of two different crystalline phases at room temperature besides the amorphous phase was concluded.[33] A low-temperature crystalline phase, characterized by *all-trans* conformations[34,35] of the side chains, disappears after heating above 60 °C, while the other phase, with a small amount of *trans* conformations, is stable at higher temperatures; the crystallinity appeared unaffected, as concluded from X-ray diffraction.[33] Further, a narrowing of the signals of the backbone carbons at 100 °C was attributed to an increased mobility associated with a transition to a smectic phase in a narrow temperature interval[33] before melting.

Here, we present quantitative ^{13}C MAS NMR experiments on two highly regioregular P3HT samples with well-defined chemical structure and molecular weight which were recently investigated by a combination of DSC and wide-angle X-ray scattering.[30] The experiments allow the quantitative distinction of alkyl side chains belonging to crystalline and amorphous parts of the chain and confirm that at higher temperatures above the phase transition mentioned before the order of the side chains even in the crystalline part of the sample is lost, while the main chains remain unaffected. These results are consistent with the scenario suggested before based on evidence of scattering experiments[30] and is in line with the qualitative results obtained by Bolognesi et al. for P3OT.[33] The NMR crystallinity determined herein quantitatively reflects the fraction of P3HT units with well-ordered side-chain arrangement, associated with the low-temperature phase I. The NMR crystallinity thus constitutes an overall minimum value that, given the usual small deviations between crystallinities derived from different methods, can be compared with DSC results of the same sample in order to derive a more reliable upper estimate of ΔH_m of P3HT to be used as a proper reference for DSC experiments. The previous estimate by Malik and Nandi[23] in fact led to underestimations of crystallinity of P3HT by about a factor of 3.

In a second set of advanced 2D DIPSHIFT NMR experiments the mobility of the main and side chains is assessed. Our results indicate clear correlations between the molecular mobility, the local conformation, and the structure of the different crystalline phases of P3HT. Finally, a first experiment on higher molecular weight material is presented for comparison. In line with DSC results, we show that higher MW samples are characterized by a lower content of ordered alkyl side chains which we attribute to a kinetic suppression of the ordering process taking place at the phase transition around 60 °C.

Table 1. Molecular Characteristics of Samples Used in This Study

	M_n/kDa	M_w/kDa	PDI (SEC)	M_n by MALDI/kDa
P3HT 3	5.2	6.0	1.15	3.2
P3HT 6	7.9	10.1	1.28	6.6

Experimental Part

Samples. Regioregular poly(3-hexylthiophene) was synthesized using the Grignard methathesis polymerization developed by McCullough et al.[36] Using this method, highly HT regioregular samples were obtained (97% as measured by ^{1}H NMR). The samples are of well-controlled molecular weight and low polydispersity, as demonstrated by the M_n and M_w determined by size-exclusion chromatography (SEC). The corresponding data are shown in Table 1. From now on, we shall address the different samples as P3HT 3 and P3HT 6, by reference to their M_n from mass spectroscopy (MALDI), since the absolute values determined by SEC are too large due to the expanded-coil conformation of the stiff P3HT chains, rendering the calibration via the hydrodynamic volume of poly(styrene) standards imprecise. The same samples were previously investigated by small- and wide-angle X-ray scattering.[30]

Figure 3 shows calorimetric data of the two samples obtained from a DSC measurement using a Diamond DSC from Perkin-Elmer. Background contributions were subtracted resulting in measuring the apparent heat capacity $c_p(T)$. While the signal around 0 °C was attributed to the glass transition, two structural transitions show up, as confirmed by temperature-dependent X-ray scattering experiments.[30] The peak around 50−60 °C is related to the transition from phase I to phase II, and the peak at higher temperatures corresponds to crystal melting. While the first peak is weaker in P3HT 6, the second becomes larger in sample P3HT 6. The fact that the melting peak changes not only the position but also the shape (i.e., higher ΔH_m) indicates that not only the thickness of the crystals but also the crystallinity increases with increasing the molecular weight. A quantitative interpretation of the DSC data in terms of crystallinity is difficult,

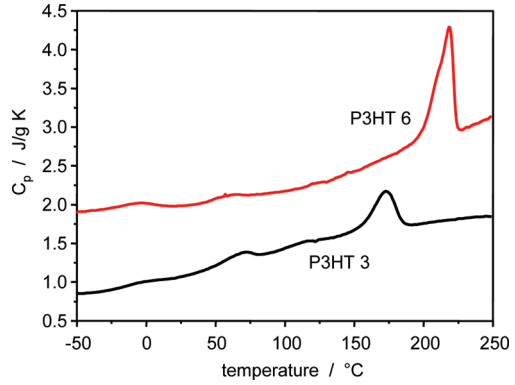

Figure 3. DSC curves for P3HT 3 (bottom) and P3HT 6 (top) as obtained during heating (20 K/min) directly after cooling to −50 °C. The enthalpies of melting as obtained by integration over the melting peak are 9.8 J/g for P3HT 3 and 20.9 J/g for P3HT 6. The data for P3HT 6 are shifted upward by 1 J/g K. Note that the melting enthalpies increase to 13.8 and 23.6 J/g, respectively, after annealing at room temperature.

given the fact that the enthalpy of melting given in the literature seems inconsistent with results from X-ray scattering and might be uncertain.[23,30] It should be noted that the melting enthalpy of both samples increases somewhat over time upon annealing at room temperature, with final values of 13.8 J/g (P3HT 3) and 23.6 J/g (P3HT 6) being reached after about 20 min.

Solid-State NMR. Three types of experiments using solid-state ^{13}C magic-angle spinning (MAS) NMR techniques were performed in order to assess the conformational state of the main and side chains, the quantitative phase composition, and the dynamics of different CH_n groups in the sample as a function of temperature. First, it is important to note that ^{13}C chemical shifts taken from simple 1D spectra are indicative of the conformation of the respective chemical moieties.[34,35] The conformational state measured in this experiment corresponds to an average on the millisecond time scale, given basically by the inverse chemical-shift span covered by the possible static conformations (about 5 ppm corresponding to 500 Hz at 100 MHz Larmor frequency). Two different schemes of excitation were used: Cross-polarization (CP) MAS NMR is well-suited for a time-efficient, yet nonquantitative acquisition of ^{13}C spectra. It is based on transferring the high polarization of protons to the initially less polarized ^{13}C. A second advantage is that the shorter T_1 relaxation time (time to reach the equilibrium spin population after excitation) of protons determines the time scale on which individual transients can be repeated. The CP process is, however, nonquantitative in that the different phases (crystalline and amorphous) are not polarized according to their mass ratio. The true phase composition, on the other hand, can be taken from integrals in fully relaxed single-pulse excitation (SPE) spectra. This takes a much longer time due to the lower ^{13}C polarization and because spectra need to be acquired with a transient repetition time (recycle delay) exceeding the rather long ^{13}C T_1. The actual T_1 values of the different CH_n moieties were determined in a second set of experiments using the method of Torchia.[37] The temperature dependence of T_1 allows a distinction between groups with molecular motion taking place either below or above the time scale given by the inverse Larmor frequency, i.e., about 100 MHz. Finally, we use an advanced 2D dipolar chemical shift correlation[38−40] (DIPSHIFT) experiment that is based on the chemically resolved ^{13}C MAS spectra. The DIPSHIFT pulse sequence affords a selective precession of nuclear spin states due to heteronuclear dipolar couplings only, while suppressing all other interactions. The final signal thus reflects the CH dipolar coupling in terms of a modulation pattern, which depends on a DIPSHIFT evolution time t_1, extending from 0 to the rotor period T_R, and going through a minimum at $t_1 = T_R/2$. Roughly, the depth of the minimum and the steepness of the modulation curve at $t_1 = 0$ and $t_1 = T_R$ reflect the exact magnitude of the coupling, which can be obtained by comparing with simulations. The full CH dipolar coupling (around 20 kHz for a rigid CH bond) is obtained if molecular motion of the CH internuclear vector is slow on the interaction time scale ($\tau_c^{-1} \ll 20$ kHz), while a fast-limit averaged CH dipolar is measured if the inverse correlation time (rate of the process) is much faster ($\tau_c^{-1} \gg 20$ kHz), typically above 100 kHz. For the latter case, the measured ratio of the experimental residual to the static-limit dipolar coupling is equal to a dynamic order S parameter that reflects the amplitude of molecular rotations and tumbling motions of the internuclear $^{13}C-^{1}H$ vector with respect to the B_0 field. The dynamic order parameter S corresponds to a time average of the second Legendre polynomial P_2 over a typical period of at least 1/(20 kHz)

$$S = \left\langle \frac{1}{2}(3\cos^2\alpha(t) - 1) \right\rangle_t \quad (1)$$

where α is the angle of a given CH vector with respect to the local symmetry axis of motion. Fast isotropic motion thus averages the dipolar coupling to zero.

NMR experiments were performed on a Bruker Avance III spectrometer, operating at the resonance frequency of 100.5 MHz, with a static field of 9.4 T. The temperature-dependent MAS experiments were performed at a spinning frequency $\omega_R/2\pi =$ 7000 Hz. The rotation frequency stability was within ±1 Hz, while the sample temperature for each spinning rate was calibrated[41] and is expected to be stable within ±0.3°. Typical lengths for the 90° pulses were 3.7 and 3.35 μs for the ^{13}C and ^{1}H, respectively, where the latter specifies the power level for TPPM (two-pulse phase modulation) dipolar decoupling. The CP contact time used in some of the experiments was 2 ms, if not specified otherwise. For all pulse sequences using CP, a recycle delay of 3 s was used, while for SPE experiments, a recycle delay of 10 s was used to ensure the equilibrium of the magnetization, as proven by the T_1 relaxation time measurements discussed below. NMR spectra were calibrated using α-glycine (176.2 ppm) as an external shift reference. For the 2D DIPSHIFT experiments,[38−40,42,43] the offset frequency during the frequency-switched Lee−Goldburg (FSLG) homodecoupling was $\Omega/2\pi = 52\,838$ Hz. Alanine and glycine were used to calibrate the DIPSHIFT modulation curves and thus to obtain references to the static-limit dipolar coupling constants of CH_n groups. Deconvolutions of spectral lines were performed with Gaussian, Lorentzian, or mixed line shape functions using the curve fit tool of the Origin software.

Results and Discussion

^{13}C SPE and CP MAS NMR Spectra. Temperature-dependent ^{13}C SPE MAS spectra of P3HT 3 recorded at 7 kHz MAS are presented in Figure 4. The resonances belonging to the main-chain carbons in the thiophene rings appear in the 140−120 ppm region. The assignment of the lines for the backbone carbons is according to refs 32 and 44. The region containing the backbone signals was scaled to equal height for all temperatures, hence the apparent difference in signal-to-noise (S/N) as compared to the alkyl regions. The repetition delay of 10 s is in fact sufficient for a quantitative observation of the alkyl carbons, while the main-chain carbons have impractically long T_1 (see below). For all temperatures, we observe a significant contribution of the amorphous phase of the polymer, which is represented by the broad background signal in the aromatic main-chain part of the spectrum, indicating conformational disorder. The exact line positions for main- and side-chain resonances obtained by spectrum deconvolution are given in Table 2.

The SPE spectrum at 25 °C exhibits two peaks for the methyl group in the aliphatic region, corresponding to the different conformations of the side chains (Table 2). The

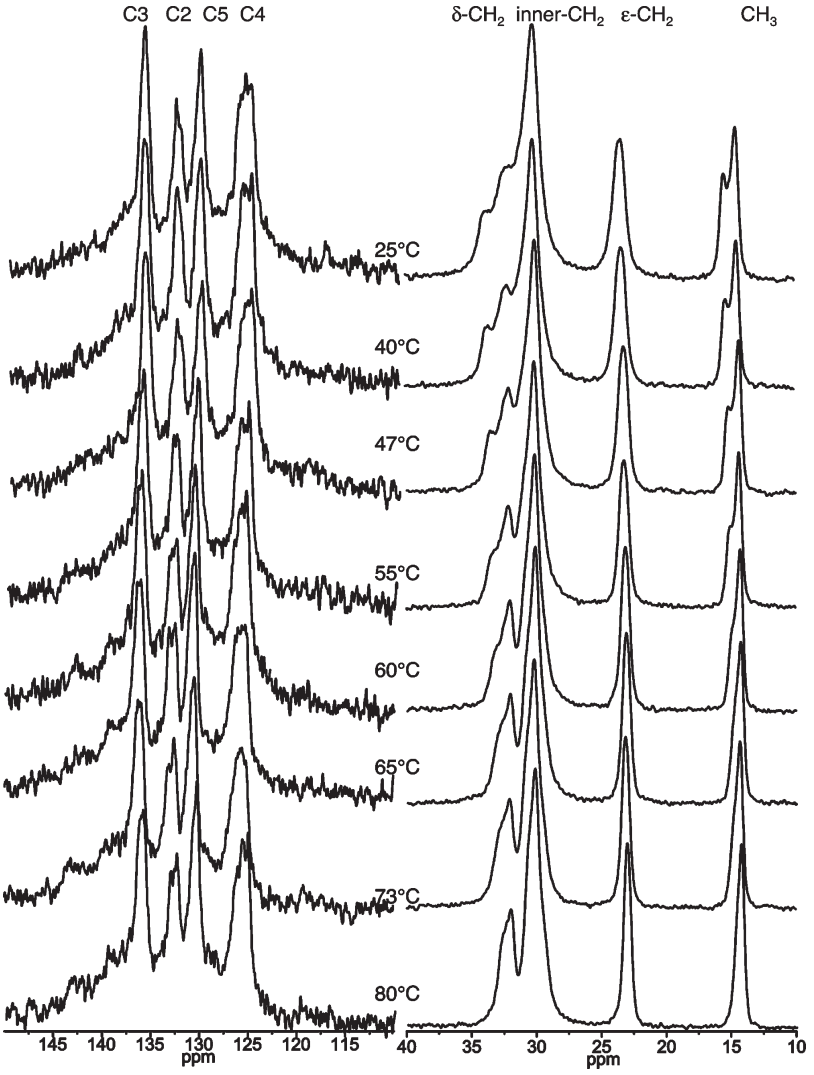

Figure 4. ^{13}C SPE MAS spectra of the P3HT 3 sample, with a recycle delay of 10 s and the temperatures indicated (spinning frequency 7 kHz).

Table 2. ^{13}C Chemical Shifts (ppm) of the Alkyl Chains in P3HT 3 from SPE MAS Spectra

T/°C	C3	C2	C5	C4	inner CH_2	ε-CH_2	CH_3
25	136.09	132.90	130.35	125.24	33.60/32.06/30.15	23.45	15.47/14.51
40	136.25	132.74	130.67	125.08	33.50/32.06/30.15	23.45	15.31/14.35
47	136.25	132.90	130.35	125.24	33.50/32.06/30.15	23.29	15.15/14.20
55	135.93	132.90	130.51	125.24	33.34/32.22/30.15	23.13	15.14/14.35
60	135.91	132.82	130.47	125.21	32.07/30.17	23.18	14.35
65	135.95	132.43	130.42	125.25	32.07/30.15	23.13	14.33
73	136.02	132.53	130.44	125.56	32.06/30.15	23.11	14.31
80	136.29	132.60	130.57	125.71	32.17/30.31	23.16	14.30

downfield peak (15.47 ppm) is associated with an average *trans* conformation at the chain end, while the upfield peak (14.51 ppm) is associated with the side chains with a higher *gauche* content.[33−35,45] Usually, one associates the chains in trans conformation with the more ordered crystalline phase (c), while the chains in a noncrystalline/amorphous phase (a) adopt more *gauche* conformations on average.

With increasing temperature, the *trans* peak of the methyl, c-CH_3, unit shifts to lower ppm values, which means that the side chains in the crystalline phase reorganize themselves from an ordered crystalline structure to a less ordered one, with increasing time-averaged *gauche* content. At and above 60 °C, the crystalline peak (now phase II) is merely a shoulder on the *gauche* peak and cannot be reliably separated any more. Below we will prove that this composite signal is indeed a superposition of carbons in different phases, i.e., the crystalline phase II and the amorphous phase.

The inner CH_2 groups resonate in the 30−33 ppm region. As detailed in Table 2, we detect three resonances in this spectral region at room temperature. According to ref 45, the α-, β-, and γ-CH_2 resonate around 29−30 ppm, while the δ-CH_2 resonance is usually shifted downfield (i.e., to high ppm). Considering that the downfield signal at 33.6 ppm behaves similarly as the trans peak of the methyl group with increasing temperature, disappearing above 60 °C, we take that this resonance rise from the inner methylenes adopting mainly *trans* conformations. The remaining signal at 32.06 ppm is assigned to δ-CH_2. It is difficult to assign the peak at 33.6 ppm to an individual methylene group; therefore, we restrict ourselves to state that this resonance represents methylenes

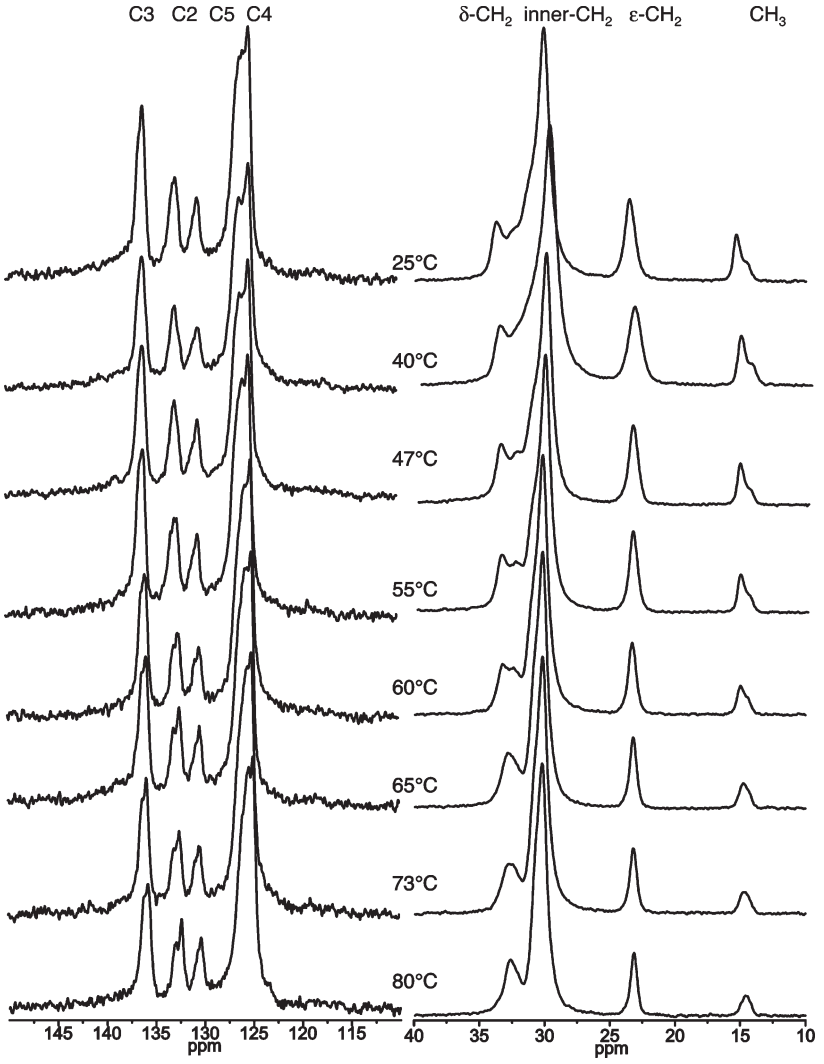

Figure 5. Temperature-dependent ^{13}C CP-MAS spectra for P3HT 3, recorded at a spinning frequency of 7 kHz and with a contact time of 200 μs; the temperature is indicated.

in mostly the *trans* configuration. The highest and broader signal at 30.15 ppm possibly represents a mix of *trans* and *gauche* conformers and is just addressed as the "inner CH_2" peak. Its overall temperature dependence is weak. The last methylenes in the side chains, ε-CH_2, resonate at 23.45 ppm; increasing the temperature leads to line narrowing and a small upfield shift.

^{13}C CP MAS spectra recorded with a short contact time (200 μs) are presented in Figure 5. Because of the short CP time used, polarization is mostly transferred over the strongest $^{1}H-^{13}C$ couplings, which means that the rigid components of the material are overemphasized. This results for instance in a significantly larger (and also temperature-dependent) *trans* signal of the CH_3 groups, and these spectra thus confirm the assignments discussed above. The fact that the aliphatic peak at 33.6 ppm is now higher and better resolved than the one at 32.06 ppm consolidates the assumption that the downfield peak belongs to methylenes with higher *trans* content.

The relative intensity of the broad background signal of the aromatic backbone, attributed to the amorphous phase, is lower than in the SPE MAS spectra, and this observation also holds for short and long CP times. This indicates that the backbone in the amorphous phase also undergoes motion at least in the range of tens of kHz and in an appreciable angular range, leading to some averaging of the associated CH dipolar couplings, explaining the lower intensity for short CP times. The fact that the signal is not much higher at longer CP suggest rather short rotating-frame spin−lattice relaxation times ($T_{1\rho}$) indicative of appreciable spectral density in the 50 kHz range (i.e., the rf frequency used for CP). Furthermore, the comparably larger broad amorphous background in the SPE spectra also indicates shorter amorphous T_1 relaxation times, which may also imply significant mobility also on the ~100 MHz scale. All interpretations corroborate the assignment of the broad background to the amorphous phase. Finally, we note that the chemical shifts of the crystalline main-chain resonances are not changing significantly with temperature, indicating that, apart from small effects induced by the changes in the average side-chain conformation, the average backbone conformation remains essentially unaffected by the crystal−crystal phase transformation.

Determination of Crystallinity and Crystal−Crystal Phase Transitions. The alkyl chain signals reflecting higher *trans* or *gauche* content in the ^{13}C MAS NMR spectra constitutes a direct way to determining the minimum crystallinity of P3HT 3. We simply integrate the quantitative respective resonances in the fully relaxed SPE spectra shown in Figure 4. The two well-resolved CH_3 resonances are best suited for this purpose and were subjected to a deconvolution analysis based

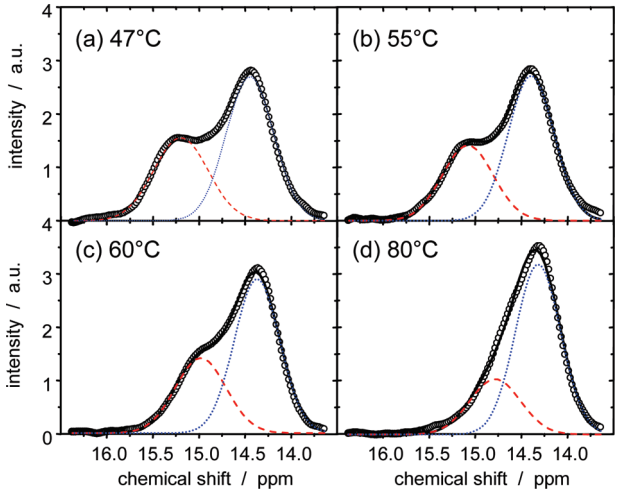

Figure 6. Component analysis of the fully relaxed ^{13}C SPE MAS NMR spectra of CH_3 in P3HT 3. Circles are the experimental data; dashed (red) and dotted (blue) lines correspond to the crystalline and mostly amorphous components, respectively, while the continuous lines are the composite line shape.

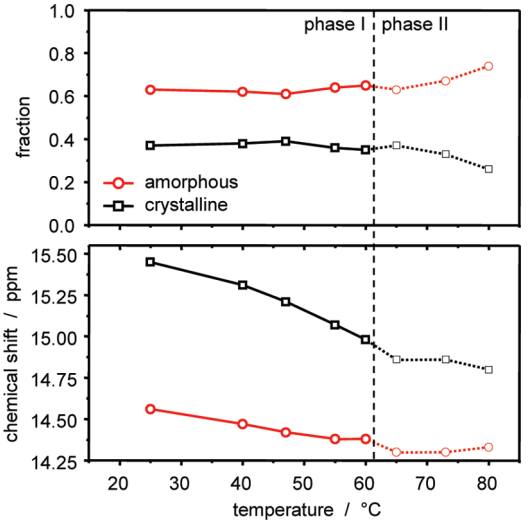

Figure 7. Crystallinity and amorphous-phase content in P3HT 3 as determined from the component analysis of the two CH_3 resonances (top) and evolution of the chemical shifts for the respective peaks as also obtained from the component analysis (bottom). The dashed line indicates the crystalline−crystalline phase transition, above which the two resonances overlap and the deconvolution becomes unstable.

on two line shape functions; the best fits of the experimental spectra were obtained with Gaussian line shapes (see Figure 6). The ratio of the integrals of the lines corresponding to the crystalline phase I and the gauche-rich (amorphous and possibly crystalline phase II) regions, respectively, directly reflects the minimum degree of crystallinity that can be attributed also to the backbone.

The crystallinity and the amorphous-phase content in P3HT 3 as determined by the component analysis are plotted as a function of temperature in the upper part of Figure 7. The averaged crystallinity detected in the low-MW sample that we investigated is 37%, with small overall variations. Note that the values are subject to potentially large systematic errors above 60 °C, where the reliability of the deconvolution procedure is limited due to the merely approximated line shape (see Figure 6d). The chemical shift data on the lower part of Figure 7 demonstrate that the average *gauche* content increases with temperature in both the crystalline and the amorphous phase, which is an expected behavior. The temperature dependence of the *gauche* content in the crystalline phase I is, however, rather strong and reflects a pretransitional phenomenon upon reaching the phase I−II transition (one may argue that the *gauche* content may serve as an order parameter in a thermodynamic sense). This transition is thus directly shown to be of dynamic nature, with the increasingly mobile side chains ultimately being responsible for a structural decoupling of adjacent 2D layers made up of well-π-packed main chains.

A crystallinity of 37% is about 2.5 times larger than the one estimated for this sample based on our DSC investigations (Figure 3). After prolonged annealing of the sample at room temperature, DSC measurements gave a heat of fusion $\Delta H_m^\infty = 13.8$ J/g (measurement not shown). A comparison with the extrapolated value for 100% crystalline material $\Delta H_m^\infty = 99$ J/g determined by Malik and Nandi would give a crystallinity of only 14%.[23] As a support, the degree of crystallinity that we determine from the NMR spectra can better explain the WAXS data for this specific sample;[30] therefore, we conclude that the literature value of ref 23 must be corrected to at most $\Delta H_m^\infty \approx 37$ J/g.

Main-Chain and Side-Chain Mobility. In this section, we will now present more quantitative results on the molecular mobility in the different phases, supporting the above conclusions and providing a detailed picture of the properties of the different phases in the material and the temperature-dependent changes. This pertains in particular to the fact that we categorized the different phases by a different time-averaged *trans* content of the alkyl resonances. Now we prove that the side chains are indeed highly (yet anisotropically) mobile in all phases, while fast backbone mobility is constrained to small angles and can be viewed as essentially rigid and unaffected by the crystal−crystal phase transformation. The mobility of the backbone has a potential effect on the efficiency of the $\pi-\pi$ packing and could thus play a role in determining the electronic properties in P3ATs. The investigation of the importance of this effect, to be evaluated against the general effect of higher crystallinity providing more effective long-range charge transport, will be the subject of future work.

Table 3. T_1 Relaxation Times (in s) Measured for P3HT 3 with Torchia's Experiment[37]

T/°C	C3	C2	C5	C4	inner CH_2	ε-CH_2	c-CH_3	a-CH_3
25	14.05	26.68	23.54	8.06	0.47	0.71	1.67	1.41
40	13.14	23.27	19.05	8.36	0.50	0.79	1.89	1.72
47	13.24	23.68	17.53	7.93	0.52	0.86	2.06	1.98
60	14.12	28.56	22.26	6.81	0.54	0.95	2.34	2.33
73	10.45	13.17	7.79	5.14	0.56	1.05	2.54	

In a second series of experiments, Torchia's CP-based T_1 spin−lattice relaxation experiment[37] was performed on the same sample for the relevant temperature range. As T_1 relaxation is mainly caused by molecular motion on the time scale of the inverse Larmor frequency, the temperature dependence of T_1 gives a qualitative account of the frequency of molecular mobility. If T_1 increases with temperature, this is attributed to faster preaveraging, i.e., the frequency of molecular motion is above the Larmor frequency. Inversely, if T_1 decreases with temperature, the frequency of molecular mobility moves into the sensitive window; i.e., the typical frequency at low temperature is below the Larmor frequency. The resulting relaxation times are presented in Table 3.

All relaxation curves could be well fitted with a single-exponential decay. The relaxation times of the alkyl signals are all below 2.5 s, proving that a recycle delay of 10 s was sufficient for quantitative SPE spectra. The T_1s of the *trans*

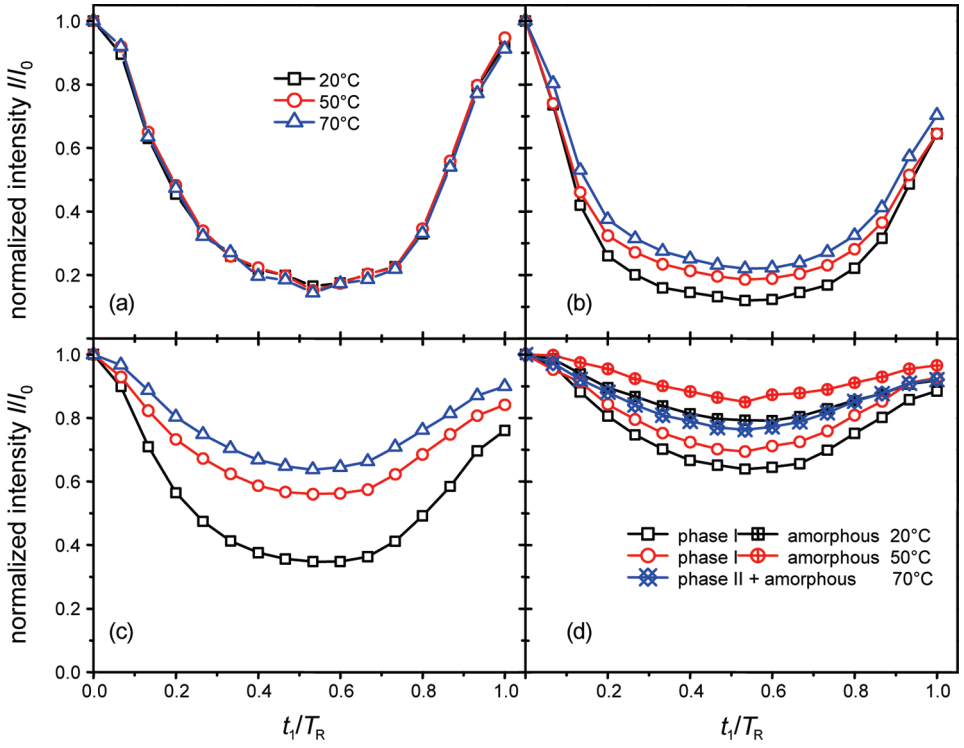

Figure 8. DIPSHIFT curves recorded in P3HT 3 sample: (a) C4 backbone, (b) inner-CH_2, (c) ε-CH_2, and (d) *trans*-rich (phase I, c) and *gauche*-rich (amorphous, a) CH_3. (a) was recorded at 4700 kHz MAS and (b)−(d) at 2500 Hz.

c-CH_3 and *gauche* peaks a-CH_3 of the methyl group are similar, becoming identical above 60 °C, where the separation of the *trans* and *gauche* configurations is not possible anymore. Both the methyl and the methylene T_1s increase with temperature, demonstrating that the conformational jump dynamics is always faster than ~100 MHz. Note the longer T_1s of the methyl groups, which arise from an effectively weak CH dipolar coupling as a result of even faster preaveraging by methyl rotation.

As expected, the T_1s of the unprotonated backbone carbons are rather long due to the lack of substantial CH dipolar couplings as the major relaxation channel. The T_1 of the protonated C4 is much longer that those of the alkyl resonances, indicating slower and/or more restricted dynamics over the whole temperature range. This value is now decreasing with temperature, placing the time scale for the small-angle librations into the branch below ~100 MHz (see the discussion of the DIPSHIFT data below for the exclusion of large-angle excursions). Note that the backbone T_1s are dominated by the crystalline phase, as a 2 ms CP was used in the experiment, for which the broad amorphous contribution is not large, in particular because the sharp signals are integrated over a narrow ppm range.

Rigidity (or a restriction to small-angle librations) is directly indicated by the magnitude of CH dipolar couplings, as obtained from the 2D DIPSHIFT experiment. In previous work,[46] we used this experiment to investigate the mobility of *trans*- and *gauche*-rich chain conformers in polymers such as poly(ethylene-*co*-acrylic acid). The principle of the method is the measurement of potentially reduced $^{13}C-^{1}H$ heteronuclear dipolar couplings D and comparing it to the static-limit value. The ratio $S = D_{exp}/D_{stat}$ (see eq 1) is a dynamic order parameter that reflects temperature-dependent changes in the degree of anisotropy of fast rotational or tumbling motions exceeding the 100 kHz range. An intensity modulation of each ^{13}C signal in the CP MAS spectrum is recorded as a function of an indirect timing variable t_1 that varies from 0 to the rotor period, T_R. For $t_1 < T_R/2$ the intensity constantly decreases, with the steepness of the decrease directly reflecting the magnitude of the $^{13}C-^{1}H$ heteronuclear dipolar coupling. For $t_1 > T_R/2$, the spectrum intensity rises again to reach its initial intensity (I_0 for $t_1 = 0$) again at $t_1 = T_R$, reflecting the time dependence of the sample rotation ("rotor echo"). Note that for higher spinning speeds the intensity modulation becomes less pronounced; therefore, weak couplings should be investigated at slower MAS. In cases where the dynamics is not in the fast limit (rate constant $k < 100$ kHz), the initial spectrum intensity is not fully recovered at $t_1 = T_R$,[47] and in such cases, the rate constant k of the motion (inverse correlation time) can be estimated.

DIPSHIFT experiments were performed at temperatures below and above the crystal−crystal phase transition of P3HT 3. The results obtained for the alkyl chains and the backbone (C4) are presented in Figure 8. The results show that in the case of the backbone (Figure 8a) the strength of the detected dipolar coupling is not changing with the temperature, which leads us to conclude that the mobility of the backbones does not change at all over this temperature range. The estimated dipolar coupling is somewhat below the expected rigid-limit value (corresponding to $S_{C4-H} = 0.79$), which is expected as this signal contains a small and apparently rather constant contribution from the more mobile amorphous regions.

For the alkyl chains, where higher mobility is expected, we used a slower spinning rate (2500 Hz) which roughly doubles the effect of the $^{13}C-^{1}H$ coupling as compared to the curves recorded with a rotation frequency of 4700 Hz. In the case of the inner-CH_2 methylenes (Figure 8b), we detect a decisive change in the amplitude of the motion with increasing the temperature from 20 to 70 °C. Comparing the size of their intensity "dip" at $T_R/2$ with those of the outer part of the chain (Figure 8c), alkyl groups in the vicinity of the thiophene ring are seen to be more restricted than the ends. Such a mobility gradient is certainly expected. Increasing the temperature and approaching the crystal−crystal phase transition

at 60 °C, the whole side chain becomes more mobile, with more pronounced changes toward the chain ends.

Note that the loss of intensity for the final points ($t_1/T_R \approx 1$) in Figure 8b−d is in this case not the result of intermediate motions in the kilohertz range. The reference experiments on rigid-CH_n model substances show the same behavior under the given experimental conditions, proving that the (weak) apparent decay is a result of radio frequency and timing imperfections at the slower MAS frequency, where more errors accumulate during the longer rotor period. Therefore, the alkyl mobility is always in the fast limit (> 100 kHz), and the changes in the data indicate that merely the amplitude of angular excursions is increasing.

For the CH_3 resonances (Figure 8d), the data indicate a difference in the mobility of the *trans*- and *gauche*-rich side chains. At room temperature, the signal from the *trans* segments in the crystalline phase I (c-CH_3) reflects a more anisotropic dynamics than the signal from the amorphous fraction (a-CH_3). Upon increasing the temperature, both populations are becoming more mobile, yet at 70 °C, where only one signal is observed, we observe a modulation that is roughly in-between the response of the separated signals at 50 °C. This is important and directly proves that the side chains in phase II are still more ordered than the amorphous side chains. The resulting overlapped signal is thus proven to be an inhomogeneous superposition of signals from two dynamically distinct phases, i.e., phase II and the amorphous phase. It should still be possible to determine the relative contributions of the two phases by studying the (potentially bicomponent) behavior of the composite signal in simple relaxation experiments or more elaborate magnetization filters. This will also be the subject of future work.

Using a custom written FORTRAN program to numerically solve the powder-averaging integral that is part of the theoretical formula describing the dipolar time modulation of the signal, we simulated the time evolution of the NMR signal under the influence of the reduced dipolar coupling in the DIPSHIFT experiment for different coupling strengths and compared them with experimental results, thus obtaining estimated values for the dipolar coupling constants. So-obtained (apparent) values always deviate from real values due to differences between simulated and real coupling topologies and due to a pulse sequence scaling factor which can differ from the theoretical value as a result of setup imperfections (radio-frequency inhomogeneities, etc.). Therefore, our fitted results were compared with analogous results obtained from fits to our experiments on rigid-limit model substances (glycine for CH_2 groups and alanine for CH_3). The ratio of these apparent couplings gives the dynamic order parameter $S = D_{exp}/D_{stat}$ with good confidence. Its expected values range from 1 (full rigidity) to 0 (isotropic motion), and the results are plotted in Figure 9.

The evolution of the order parameters with temperature fully confirms the above qualitative interpretation. It is important to emphasize the meaning of the apparent increase of S detected on the gauche-rich CH_3 signal at the highest temperature (70 °C), which can only be explained by the fact this signal is now a superposition of the amorphous phase (for which $S \approx 0.25$ could be estimated; see dotted line in Figure 9) and the newly formed phase II. The high value of ~0.48 at 70 °C is consistent with the mobility in phase II being not much higher (if at all) than in phase I, yet with higher *gauche* content on average, as inferred from the signal position. This indicates a structural rearrangement accommodating more side-chain conformers, which is consistent with the observations from X-ray scattering.[30] Certainly, the disordering observed in NMR explains perfectly the X-ray

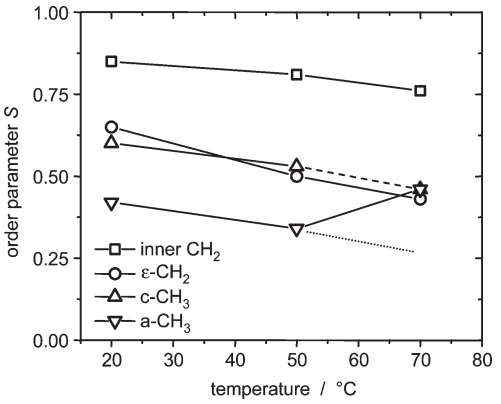

Figure 9. Order parameter S for the P3HT side chains versus temperature. The dashed line indicates that the c-CH_3 peak moves under the a-CH_3 peak, and the dotted line indicates a possible trend for the pure amorphous phase.

results, namely a loss of position correlation between different layers of main chains. As for absolute values, $S > 0.5$ for the last ε-CH_2 group in fact excludes a full rotational motion of the chain, as is for instance found in hexagonal rotator phases of long alkanes. Since the CH dipolar vectors are on average perpendicular to the expected symmetry axis of motion (= extended side-chain axis), a reduction by at least 50% would be expected for that case. Note that a simple 180° jump motion around the extended-chain axis conserves the dipolar tensor orientation and would not lead to any apparent dynamic averaging. We can thus conclude that the chain end performs conformational jumps over a limited set of positions, with possibly some additional librations.

While all together the results are in line with the conclusions drawn from X-ray scattering, there is detailed information obtained by NMR that goes much beyond. Side-chain mobility depends on the position on the side chain with the most mobile parts being at the chain ends. Also, the temperature dependence seems rather smooth in the small temperature interval of the experiment. Additionally, there is some information available about the absolute time scale of molecular motion of the different molecular groups; most importantly, there is a strong mobility difference between main and side chain.

Effect of M_n on Chain Mobility and Crystallinity. Several studies showed that the mobility of charge carriers in P3HT increases with increasing molecular weight of the sample.[8−13] We have thus investigated the P3HT 6 sample with a higher molecular weight (see Table 1), which exhibits a substantially increased crystallinity as judged from DSC, in order to investigate the effect of molecular weight on the main/side chain mobility and the NMR-detected phase distribution. Both the CP and SPE MAS spectra at different temperatures show no relevant differences as compared to those recorded for the P3HT 3. P3HT 6 features slightly sharper lines for the main and side chains, and this difference could arise from either an increased mobility and/or a more ordered structure.

The only very relevant difference is found for the side-chain CH_3 signals at lower temperature, as shown in Figure 10. Obviously, the amount of alkyl-ordered phase I is lower in the higher MW sample, which is at a first glance in contradiction to the higher DSC estimate of crystallinity. Using our deconvolution procedure for SPE spectra, we find a phase I fraction of 28%, which should be compared to 37% for P3HT 3. This apparent contradiction can be resolved by taking into account that in the DSC scan for the higher MW

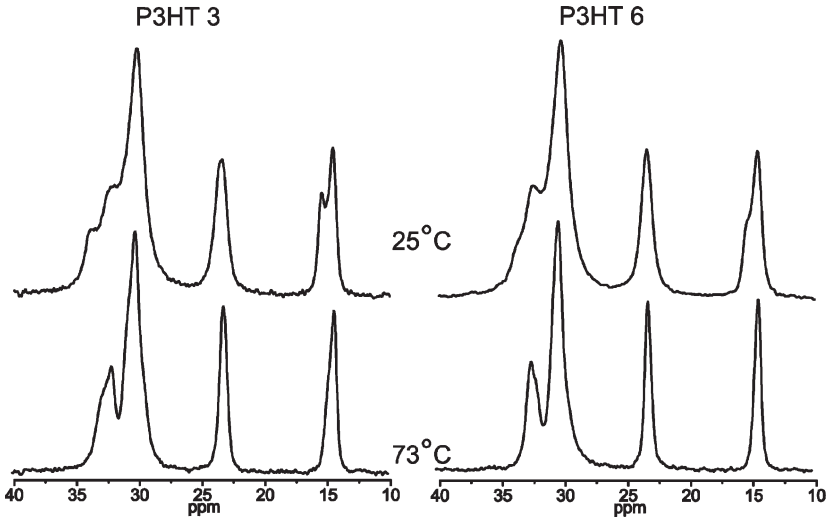

Figure 10. SPE MAS spectra (aliphatic region) of P3HT 3 and P3HT 6 at two relevant temperatures.

(Figure 3) the endotherm at around 60 °C is less visible (it in fact almost vanishes for even higher MW, data not shown). This phenomenon has been interpreted as a result of a kinetic suppression of the phase I formation on cooling for high molecular weights in the context of our X-ray scattering results.[30] This assumption is here confirmed on a molecular basis and demonstrates that our "NMR crystallinity," more precisely the phase I content, is only a lower limit. Also in P3HT 3, we cannot fully exclude some regions that do not transform into phase I. These issues will be addressed in future annealing studies. Note that our crystallinity estimates for the two samples correspond to extended annealing at room temperature, yet changes may be possible by annealing at elevated temperature, e.g., around the phase I−phase II transition or just below melting.

Independent proof of our interpretation that the higher MW material is rich in phase II already at room temperature is again inferred from the mobility information obtained from the DIPSHIFT experiment. Figure 11 shows the modulation curves for the backbone C4 as well as the *gauche*-rich methyl resonance (a-CH_3), all recorded at a spinning rate of 4700 Hz. The full symbols are data recorded for the sample with the lowest molecular weight (P3HT 3) while the empty symbols are for P3HT 6 sample. The faster MAS leads to less pronounced modulations of the CH_3 signal as compared to Figure 8d; however, together with the higher DSC crystallinity, the conclusion is clear: the higher MW sample shows a significantly more pronounced modulation, indicating that the a-CH_3 signal is in fact a superposition of most mobile amorphous regions and phase II with lower local mobility. This is consistent with a kinetically suppressed phase transition; i.e., molecular motion is too slow to develop order without prolonged annealing.

Further, the temperature independence of the backbone C4 response again demonstrates that the temperature-dependent side-chain mobility as well as a partial crystal−crystal phase transition at around 50−60 °C does not affect the dynamics of the main chain at all. The even stronger modulation observed for P3HT 6, corresponding to $S_{C4-H} = 0.92$, can straightforwardly be explained by an even lower contribution of underlying (more mobile) amorphous signal components, in agreement with the higher crystallinity. The modulation is even closer to rigid-limit behavior, suggesting that the fast C4−H bond fluctuations (that do exist and are the reason for its T_1 relaxation behavior) are constrained to rather small angles. The finding also shows that the side-chain

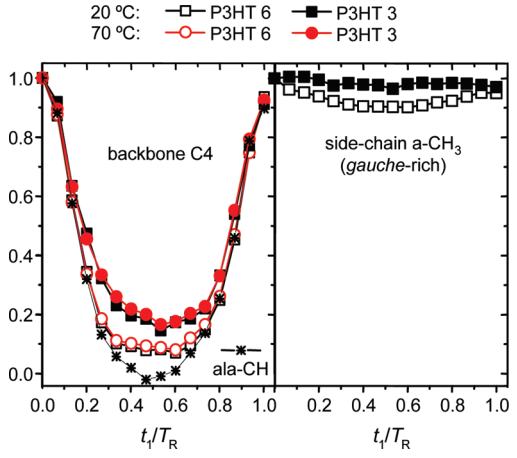

Figure 11. DIPSHIFT curves of C4 and a-CH_3 for P3HT with different MW and at different temperatures. The stars in the C4 plot on the left are for the alanine CH group, corresponding to complete rigidity.

mobility (which is higher in P3HT 6 with its higher phase II content) does not significantly affect the backbone rigidity.

Assuming for a moment a negligible contribution of the broad amorphous background, the difference between the two samples could then be explained by a difference in the angular range of the fluctuations on the given time scale, which would mean that the higher crystallinity, along with the larger lamellar thickness, leads to a better packing in a more ordered structure as in the lower molecular weight. An investigation into whether this effect is relevant for electronic transport will be a central subject of our future work.

Conclusions

Structure, dynamics, and crystallinity at moderate temperatures in two highly HT-regioregular P3HT samples were investigated using ^{13}C MAS NMR spectroscopy and DSC. DSC measurements show a crystal−crystal phase transition around 60 °C. Based on X-ray scattering results, the transition was suggested to correspond to a transition from a well-organized 3D crystalline structure (phase I) in which the side chains are well ordered to a 2D crystalline structure (phase II), where the side chains are more mobile and have a high *gauche* content but are still less mobile than in the amorphous phase. For the higher molecular weight this transition is weaker while a higher melting enthalpy indicates a higher overall crystallinity. This picture could be fully confirmed

by NMR measurements showing the expected differences in molecular mobility in the different molecular regions. Regarding the absolute crystallinity, using literature data[23] for the reference melting enthalpy, the expected crystallinity in the P3HT 3 sample would be around 14%. Quantitative ^{13}C NMR yields a phase I content of 37% which represents a minimum value for the crystallinity, leading to a corrected maximum reference value for the melting enthalpy of $\Delta H_m^\infty \approx 37$ J/g and proving the literature value incorrect. Taking this value for calibration of the other material, P3HT 6 has a crystallinity of about 64%. Such substantial crystallinities in P3HT were as yet not reported, and this knowledge is essential for discussions about the effect of crystallinity on the charge carrier mobility in poly(3-alkylthiophenes) in general.

NMR experiments focusing on the angular range of fast reorientations of CH bonds were used to monitor the mobility of the main and side chains with chemical resolution below and above the crystal−crystal phase transition at 60 °C. These results reveal that the mobility and the average conformation of the main chains is neither affected by temperature nor by the crystal−crystal phase transition; however, in the side chains, an increasing degree of mobility and a reorganization of the chain ends toward on average conformations with higher gauche content in phase II are indicated. Experiments on a sample with higher molecular weight show that the crystal−crystal phase transition from phase II to phase I on cooling is kinetically suppressed, meaning that at room temperature higher MW material is predominantly in phase II, while the backbones are on average even less mobile. The known better device performance, i.e., the higher charge carrier mobility in samples with larger molecular weight, is thus shown to correlate with absolute crystallinity, highlighting a way to possibly further improve these materials.

On the methodological side, we point out again that the used NMR methods, sensitive to local structure and mobility, proved indispensable in confirming the structural model that was previously suggested, but could not be proven on the sole basis of diffraction data. Such a combined approach is especially useful for materials such as the present one, which, despite being made up of homopolymers, form complex nanoscopic structures and exhibit pronounced dynamic heterogeneity even within the crystalline phase(s). The present investigation concentrated on fast dynamics of the main and side chains, yet other authors proved that the backbones exhibit a slower dynamics (slow conformational jumps), as accessible by exchange NMR spectroscopy methods.[32] Such processes could also be relevant for the device performance, as they directly affect the $\pi-\pi$ packing. Investigations regarding the slow dynamics in the backbones, as well as aging studies focusing on changes in the phase I/II composition of our well-defined P3HT samples, and on practically relevant thin-film samples are ongoing.

Acknowledgment. This work was supported by the Deutsche Forschungsgemeinschaft (SPP 1355) and the state of Saxony-Anhalt. We acknowledge infrastructural support from the European Union (ERDF programme) and further thank K. Herfurt for technical help with the DSC experiments.

References and Notes

(1) Forrest, S. *Nature* **2004**, *428*, 911.
(2) Li, G.; Shrotriya, V.; Huang, J.; Yao, Y.; Moriarty, T.; Emery, K.; Yang, Y. *Nature Mater*. **2005**, *4*, 864.
(3) Kim, Y.; Cook, S.; Tuladhar, S.; Choulis, S.; Nelson, J.; Durrant, J.; Bradley, D.; Giles, M.; McCulloch, I.; Ha, C.; Ree, M. *Nature Mater*. **2006**, *5*, 197.
(4) Roncali, J. *Chem. Rev*. **1997**, *97*, 173–205.
(5) Sirringhaus, H.; Brown, P. J.; Friend, R. H.; Nielsen, M. M.; Bechgaard, K.; Langeveld-Voss, B. M. W.; Spiering, A. J. H.; Janssen, R. A. J.; Meijer, E. W.; Herwig, P.; de Leeuw, D. M. *Nature* **1999**, *401*, 685–688.
(6) Xu, B.; Holdcroft, S. *Macromolecules* **1993**, *23*, 4457–4460.
(7) Bao, Z.; Dodabalpur, A.; Lovinger, A. J. *Appl. Phys. Lett*. **1996**, *69* (26).
(8) Kline, R. J.; McGehee, M. D.; Kadnikova, E. N.; Liu, J.; Fréchet, J. M. J.; Toney, M. F. *Macromolecules* **2005**, *38*, 3312–3319.
(9) Brinkmann, M.; Rannou, P. *Macromolecules* **2009**, *42*, 1115–1130.
(10) Kline, R. J.; McGehee, M. D. *Adv. Mater*. **2003**, *15*, 1519–1522.
(11) Goh, C.; Kline, J.; McGehee, M. D.; Kadnikova, E. N.; Fréchet, J. M. J. *Appl. Phys. Lett*. **2005**, *86*, 122110.
(12) Zen, A.; Pflaum, J.; Hirschmann, S.; Zhuang, W.; Jaiser, F.; Asawapirom, U.; Rabe, J. P.; Scherf, U.; Neher, D. *Adv. Funct. Mater*. **2004**, *14*, 757–764.
(13) Esenturk, O.; Melinger, J. S.; Heilweil, E. J. *J. Appl. Phys*. **2008**, *103*, 023102.
(14) Zen, A.; Saphiannikova, M.; Neher, D.; Grenzer, J.; Grigorian, S.; Pietsch, U.; Asawapirom, U.; Scherf, U.; Lieberwirth, I.; Wegner, G. *Macromolecules* **2006**, *39*, 2162–2171.
(15) Joshi, S.; Grigorian, S.; Pietsch, U.; Pingel, P.; Zen, A.; Neher, D.; Scherf, U. *Macromolecules* **2008**, *41*, 6800–6808.
(16) Joshi, S.; Grigorian, S.; Pietsch, U. *Phys. Status Solidi A* **2008**, *205* (3), 488–496.
(17) McCullough, R. D. *Adv. Mater*. **1998**, *10*, 93–116.
(18) Mao, H.; Xu, B.; Holdcroft, S. *Macromolecules* **1993**, *23*, 1163–1169.
(19) McCullough, R. D.; Tristram-Nagle, S.; Williams, S. P.; Lowe, R. D.; Jayaraman, M. *J. Am. Chem. Soc*. **1993**, *115*, 4910–4911.
(20) Chen, T.-A.; Wu, X.; Rieke, R. D. *J. Am. Chem. Soc*. **1995**, *117*, 233–244.
(21) Sheina, E. E.; Liu, J. S.; Iovu, M. C.; Laird, D. W.; McCullough, R. D. *Macromolecules* **2004**, *37*, 3526–3528.
(22) Pankaj, S.; Hempel, E.; Beiner, M. *Macromolecules* **2009**, *42*, 716–724.
(23) Malik, S.; Nandi, A. K. *J. Polym. Sci., Part B: Polym. Phys*. **2002**, *40*, 2037–2085.
(24) Prosa, T. J.; Winokur, M. J.; Moulton, J.; Smith, P.; Heeger, A. J. *Macromolecules* **1992**, *25*, 4364–4372.
(25) Brinkmann, M.; Wittmann, J.-C. *Adv. Mater*. **2006**, *18*, 660–863.
(26) Prosa, T. J.; Winokur, M. J.; McCullough, R. D. *Macromolecules* **1996**, *29*, 3654–3656.
(27) Kline, R. J.; DeLongchamp, D. M.; Fischer, D. A.; Lin, E. K.; Richter, L. J.; Chabinye, M. L.; Toney, M. F.; Heeney, M.; McCulloch, I. *Macromolecules* **2007**, *40*, 7960–7965.
(28) Chen, T.-A.; Rieke, R. D. *J. Am. Chem. Soc*. **1992**, *114*, 10087–10088.
(29) Barbarella, G.; Bongini, A.; Zambianchi, M. *Macromolecules* **1994**, *27*, 3039–3045.
(30) Wu, Z.; Petzold, A.; Henze, T.; Thurn-Albrecht, T.; Lohwasser, R.; Sommer, M.; Thelakkat, M. *Macromolecules* **2010**, *43*, 4646–4653.
(31) Ferrari, M.; Mucci, A.; Schenetti, L. *Magn. Reson. Chem*. **1995**, *33*, 657–663.
(32) Yazawa, K.; Inoue, Y.; Yamamoto, T.; Asakawa, N. *Phys. Rev. B* **2006**, *74*, 094204.
(33) Bolognesi, A.; Porzio, W.; Provasoli, A.; Botta, C.; Comotti, A.; Sozzani, P.; Simonutti, R. *Macromol. Chem. Phys*. **2001**, *202*, 2586–2591.
(34) Tonelli, A. E. *Macromolecules* **1978**, *11*, 565–567.
(35) Earl, W. L.; VanderHart, D. L. *Macromolecules* **1979**, *12*, 762–767.
(36) Sheina, E. E.; Liu, J.; Iovu, M. C.; Laird, D. W.; McCullough, R. D. *Macromolecules* **2004**, *37*, 3526–3528.
(37) Torchia, D. A. *J. Magn. Reson*. **1978**, *30*, 613.
(38) Hong, M.; Gross, J. D.; Griffin, R. G. *J. Phys. Chem. B* **1997**, *101*, 5869–5874.
(39) Munowitz, M. G.; Griffin, R. G. *J. Chem. Phys*. **1981**, *76* (6), 2848.
(40) Harris, R. K.; Jackson, P.; Merwin, L. H.; Say, B. J.; Hägele, G. *J. Chem. Soc., Faraday Trans. 1* **1988**, *84* (11), 3649–3672.
(41) Bielecki, A.; Burum, D. P. *J. Magn. Reson*. **1995**, *A116*, 215–220.
(42) Hester, R. K.; Ackerman, J. L.; Neff, B. L.; Waugh, J. S. *Phys. Rev. Lett*. **1976**, *36* (18), 1081–1083.
(43) Schaeffer, J.; McKay, R. A.; Stejskal, E. O. *J. Magn. Reson*. **1983**, *52*, 123–129.
(44) Barbarella, G.; Casarini, D.; Zambianchi, M.; Favaretto, L.; Rossini, S. *Adv. Mater*. **1996**, *8*, 69–73.
(45) VanderHart, D. L. *J. Magn. Reson*. **1981**, *44*, 117–125.
(46) Meyer, C.; Pascui, O. F.; Reichert, D.; Sander, L. C.; Wise, S. A.; Albert, K. *J. Sep. Sci*. **2006**, *29*, 820–828.
(47) deAzevedo, E. R.; Saalwachter, K.; Pascui, O. F.; de Souza, A. A.; Bonagamba, T. J.; Reichert, D. *J. Chem. Phys*. **2008**, *128*, 104505.